Impact of residential low-carbon technologies on low-voltage grid reinforcements

Simon Meunier, Christina Protopapadaki, Ruben Baetens, Dirk Saelens

Impact of residential low-carbon technologies on low-voltage grid reinforcements

Simon Meunier[1,2,*], Christina Protopapadaki[1,2], Ruben Baetens[3], Dirk Saelens[1,2]

[1]KU Leuven, Department of Civil Engineering, Building Physics Section, Kasteelpark Arenberg 40, Heverlee 3001, Belgium

[2]EnergyVille, Thor Park 8310, Genk 3600, Belgium

[3]3E, Kalkkaai 6, Brussels 1000, Belgium

*Corresponding author at: KU Leuven, Department of Civil Engineering, Building Physics Section, Kasteelpark Arenberg 40, Heverlee 3001, Belgium, simon.meunier@kuleuven.be (Simon Meunier)

Abstract:

Integrating low-carbon technologies (e.g. heat pumps, photovoltaic systems) in buildings influences the stability of the low-voltage grid, which therefore often requires to be reinforced. This article proposes a techno-economic methodology to identify the reinforcements needed to maintain grid stability at the lowest life-cycle cost. Novel contributions include the consideration of three-phase connection of low-carbon technologies as a reinforcement option and the fact that we study to what extent grid reinforcements can mitigate voltage unbalance issues. Additionally, to reduce computing time, a *dummy island* approach is used, whereby one feeder is modelled in detail and the remainder of the distribution island is represented by an aggregated load. Finally, random repetitions are proposed, to consider uncertainties related to building properties, occupants and the location of low-carbon technologies in the feeders. The methodology is applied to investigate the integration of heat pumps and photovoltaic systems in typical Belgian rural and urban grids. For the rural grid, heat pumps may lead to significant reinforcement costs (up to 1230 €/dwelling), mainly due to voltage stability problems. For the urban grid, heat pump and photovoltaic integration causes low reinforcement cost (< 200 €/dwelling). Furthermore, more random repetitions are required to obtain robust results for the rural grid than for the urban one. The proposed methodology is generic and transferrable to other radial low-voltage grids and low-carbon technologies (e.g. electric vehicles). It can help grid operators and policy makers integrate low-carbon technologies in a more resilient and cost-effective way, by weighing their available grid reinforcement solutions.

Highlights:

- Residential low-carbon technologies integration in low-voltage grids is analysed.
- A generic methodology to compute the grid reinforcement cost is developed.
- High-resolution Modelica simulations are performed for Belgian dwellings and grids.
- Heat pump integration in rural grid costs up to 1230 €/dwelling for reinforcement.
- Less than 200 €/dwelling reinforcement cost for integration in urban grid.

Keywords: Low-voltage grids, Distributed energy systems, Heat pumps, Photovoltaic systems, Techno-economic analysis

Nomenclature

Abbreviations

DSO	distribution system operator
HP	heat pump
LCT	low-carbon technology
LV	low-voltage
MV	medium-voltage
PV	photovoltaic
RES	renewable energy sources
UK	United Kingdom

Indices

d	dwelling
dc	dwelling connection
dl	dwelling link
fs	feeder segment
j	phase index
k	position in the feeder
n	node
t	time
τ	transformer

Variables

b_f	feeder replacement binary variable
b_τ	transformer replacement binary variable
$b_{3\phi}(d)$	3-phase connection binary variable
$E_l(\tau)$	yearly energy losses in the transformer (kWh)
$E_l(f)$	yearly energy losses in the detailed feeder (kWh)
$fl(fs)$	overloading of feeder segment
$FL(fs)$	overloading indicator of the feeder segment
FL	overloading indicator for the whole feeder
$i(dl)$	current in dwelling link (A)
$i(fs)$	current in feeder segment (A)
$i(\tau^j)$	current in phase j of the transformer (A)
IC	investment cost associated to a reinforcement option (€)
LCC_d	life-cycle cost per dwelling associated to a reinforcement option (€)
LCC_d^*	cost of the cheapest technically viable reinforcement option (€)
OC	operating costs associated to a reinforcement option (€)
ρ	number of random repetitions
$S(\tau)$	apparent power through the transformer (kVA)
$tl(\tau)$	transformer overloading
TL	transformer overloading indicator
$v(dc_k^j)$	line-to-neutral voltage at the dwelling connection in position k and for phase j (V)
$v(n_k^{j,j'})$	line-to-line voltage at the node in position k between phases j and j' (V)
$VD(d_k)$	voltage deviation indicator for the dwelling in position k
VD	voltage deviation indicator for the whole feeder
$vu(n_k)$	voltage unbalance at the node in position k
$VU(n_k)$	voltage unbalance indicator at the node in position k
VU	voltage unbalance indicator for the whole feeder

Parameters

$C(E_l)$	cost per kWh of energy losses for the DSO (€/kWh)
$C(\tau)$	cost of replacing the existing transformer by a new transformer τ (€)

$C_l(dl)$	linear cost of replacing the current one-phase dwelling link by a three-phase cable (€/m)
$C_l(f)$	linear cost of replacing the existing feeder cables by new ones (€/m)
C_r	cost of reconnecting a dwelling link to the feeder (€)
$C_{3\phi,m}$	cost of a three-phase meter (€)
D_f	number of dwellings in the detailed feeder
D_i	number of dwellings in the island
δ	discount rate
$i_{nom}(fs)$	current carrying capacity of the feeder segment (A)
$l(dl)$	dwelling link length (m)
$l(fs)$	feeder segment length (m)
$l_a(f)$	average length between feeder nodes (m)
$l_t(f)$	feeder length (m)
L	lifetime, i.e. planning horizon for grid reinforcements (years)
lim	limit set on the variation of the cost to establish the robustness of the results
$P_0(\tau)$	transformer no-load losses (kW)
$R(\tau^j)$	real part of the phase impedance of the transformer (Ω)
$R_l(dl)$	linear resistance of the dwelling link (Ω/m)
$R_l(fs)$	linear resistance of the feeder segment (Ω/m)
ρ	number of random repetitions
ρ_{conv}	number of repetitions without significant variation of the cost required to establish the robustness of the results
$S_{nom}(\tau)$	nominal capacity of the transformer (kVA)

1 Introduction

In the residential sector, a large-scale deployment of low-carbon technologies (LCTs), such as photovoltaic (PV) systems, heat pumps (HPs) and electric vehicles, is required to decrease greenhouse gas emissions [1]. However, the integration of these renewable energy sources (RES) and new loads in buildings has a strong impact on the stability of the low-voltage (LV) grid, namely causing cable and transformer overloading, voltage deviations from the nominal, voltage unbalance, and harmonic distortion, among others [2] [3]. Solving these problems is often done by reinforcing the grid [4] [5]. Other solutions in literature propose making use of the flexibility that systems such as heat pumps and electric vehicles can offer [6] [7]. However, the latter options require appropriate communication infrastructure and controls. Even though literature has been increasingly studying these options, technical, economic and regulatory challenges remain [8] [9], as well as uncertainties related to the willingness of households to participate in demand response programs [10]. It is therefore of key importance to identify the necessary grid reinforcements for the integration of LCTs, and to provide an assessment of their cost. In this way, meaningful comparisons can be made as to which solutions are more cost effective, which could facilitate the development of energy policies.

1.1 Literature review

Grid reinforcement for LCT integration has been the focus of several studies. Certain articles investigated the influence of RES integration in buildings on the required grid reinforcements. The influence of PV integration has been investigated in case studies in the United Kingdom (UK) [11], Switzerland [12], Germany [13] [14] [15], Australia [16] and the United States [17] [18]. The grid stability indicators considered in these studies were voltage deviation as well as transformer and feeder overloading. The reinforcement options investigated to maintain grid stability were limited to transformer and feeder replacement. Other literature focused on network reinforcements related to the integration of new electrical loads instead. Cases of electric vehicle integration were investigated in studies in Italy [19], Denmark [20], Germany [20], the Netherlands [20] and the UK [21]. The effect of a combined integration of HPs and electric vehicles for a UK LV grid was the focus of study [22]. As for RES, overloading and voltage deviations were examined in these studies, with transformer and feeder cable replacement as reinforcement options.

Finally, some articles studied the necessary grid reinforcements to facilitate the joint integration of RES and new electrical loads. In [23], the effectiveness of reinforcement options was investigated to mitigate voltage deviation and unbalance issues triggered by PV generation and electrical loads increase. However generic load profiles from 1997 [24] were used in this study. Furthermore, the cost of grid reinforcement options is not considered, which prevents from comparing two technically viable options. Finally, PV generation and load increase are considered separately, which does not allow identifying effects of combined integration on grid stability and on the adapted reinforcements. In other works performed for the UK, the required distribution grid reinforcements and

associated cost for PV and HP deployment [25], and for PV integration and load growth [26] were investigated. Brinkel et al. focused on the integration of PV systems and electric vehicles in Dutch grids [27]. Morjav et al. studied the combined integration of HPs, PV systems and CHP (combined heat and power) into the IEEE European Low Voltage Test Feeder [28] [29]. They identified the reinforcement options (transformer and/or line replacement) for mitigating voltage deviation and overloading at the lowest cost [29].

1.2 Research gaps, contributions to the research field and article structure

Analysis of the above literature allows drawing attention to several aspects that are insufficiently addressed in articles that investigate grid reinforcements for the integration of LCTs. First, most articles did not investigate the benefit of grid reinforcement on the mitigation of voltage unbalance, even though voltage unbalance is one of the main problems that may occur with LCT deployment [2]. To our best knowledge, the only exception is the conference article [23], which however lacked economic assessment, realistic and up-to-date electrical loads and the consideration of combined new loads and RES deployment, as already mentioned. Additionally, none of the above studies considers the possibility of connecting new loads and distributed generation sources to three phases instead of one as a reinforcement option, although it may efficiently contribute to voltage stability [30]. We also observed that the methodologies used in previous articles rely on detailed simulations of the entire LV island, which can lead to large computation times. This may limit the scope of the analysis to few specific case studies and scenarios, not allowing for a probabilistic assessment. Finally, for each LCT integration rate, current articles only provide the cost of the cheapest technically viable reinforcement option. However, examining the grid stability indicators and cost for all reinforcement options and all LCT integration rates would help better understanding the effectiveness of each option in relation to its cost. Moreover, it would allow evaluating the suitability of grid reinforcement options for different levels of LCT integration, and identifying which options may become unviable once a given level of integration is reached.

In this article, we propose a methodology for grid reinforcement analysis that addresses the identified shortcomings in literature. It allows identifying the reinforcement options that are the most technically and economically efficient in tackling grid stability problems triggered by the integration of new electrical loads and distributed generation sources. For this methodology, we developed a detailed technical model that simulates the influence of LCT integration scenarios and grid reinforcement options on four grid stability indicators. The technical model incorporates occupant behaviour, captures the thermal response of the buildings and allows 3-phase unbalanced load flow calculations. This bottom-up approach is flexible, and it allows for an accurate assessment of the grid impacts. Contrarily to existing studies, our technical model allows considering voltage unbalance as a grid stability indicator and the possibility to connect LCTs to three phases as a grid reinforcement option. Another difference of our method compared to literature is the use of the *dummy island* approach for the grid representation instead of explicitly modeling the entire LV island. In the *dummy island* approach, one feeder is modelled in detail and the remainder of the island is represented by an aggregated load [31]. This approach allows determining component loading and voltage quality, but it requires less grid input parameters and significantly reduces computing time with only a small accuracy loss [32]. Therefore, for a given LCT integration rate, we are able to simulate in a reduced time a large number of random repetitions, for each of which the occupants, buildings and repartition of LCTs on the detailed feeder vary, thus improving the robustness of the results. Finally, we also proposed an economic model that computes the life-cycle cost, which includes the cost of investment and operation of the LV grid, associated with a grid reinforcement option.

The proposed methodology is further applied to investigate the cost and viability of reinforcement options for the combined integration of HPs and PV systems in typical rural and urban LV grids of Belgium. The detailed technical model represents typical Belgian households, dwellings and LV networks, while cost data were obtained from a local distribution system operator (DSO). We study the grid stability indicators and the cost for each LCT integration rate and reinforcement option. Finally, we propose a procedure to investigate the influence that the number of random repetitions has on the robustness of our results.

The remainder of this article includes a detailed description of our methodology in Section 2. This section details the dummy island approach, the reinforcement options considered, the technical model and the associated grid stability indicators. Furthermore, the economic model is presented, which allows computing the life-cycle cost associated to a grid reinforcement option. Section 3 focuses on the application of the methodology to typical Belgian feeders, presenting the chosen dwelling and grid parameters and discussing the results regarding PV and HP integration. Section 4 presents the perspectives to our work.

2 Methodology

2.1 Overview

2.1.1 Grid architecture

In this article, we consider three-phase four-wire radial grids in star configuration, which are common in residential LV grids [33] [34], with the architecture presented in Figure 1 [31] [32]. In this architecture, the feeder of interest is modelled in detail, while the remainder LV distribution island is represented by an aggregated balanced load [31] [32]. This *dummy island* approach permits to focus on the details of a specific feeder, while also considering loads and RES in the remaining island and assessing the transformer loading and the voltage drop at the transformer due to the remainder of the island. This approach was shown to generate small deviations in electrical simulation results compared to full island simulations (simulating all feeders of the island in detail) with significant reductions in computing time [31] [32]. For instance, for the wide variety of LV islands considered in [31], using the dummy island approach instead of the full island provided around 10-fold reduction in computing time while triggering errors always smaller than 0.03, 0.01 and 0.01 pu on extreme voltage, current and transformer loading respectively.

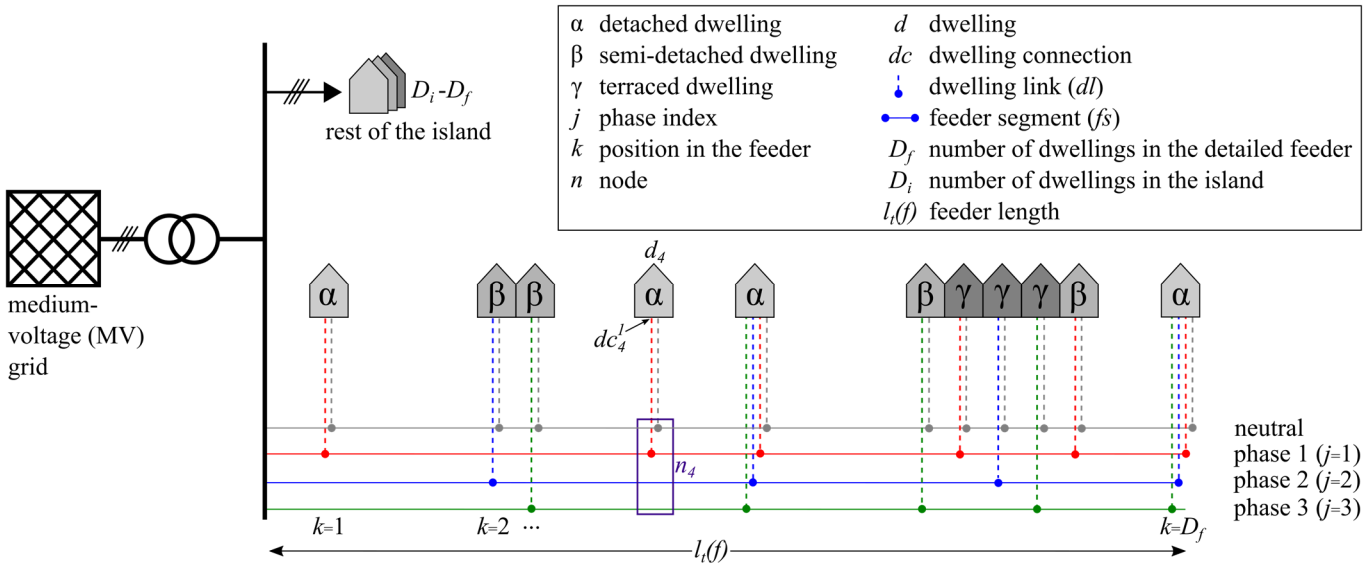

Figure 1 – Architecture of the LV grid (also called LV distribution island).

2.1.2 Low-carbon technology integration scenarios and grid reinforcement options

An *LCT integration scenario* is defined by the percentage of each LCT that is integrated in the detailed feeder. The dwellings that receive each LCT are chosen randomly. We also assume that the integration rate is the same in the rest of the island as in the detailed feeder. For instance, an LCT integration scenario with 20% HPs and 40% PV systems would correspond to 20% of the dwellings of the detailed feeder and of the island having a HP, and 40% having PV systems. Some of the dwellings may have several types of LCTs, for instance both a HP and a PV system.

The *reinforcement options* are defined relative to the initial grid. The initial grid is designed to have a feeder cable and transformer that satisfy the loads when no LCTs are applied, with all buildings having a single-phase connection to the feeder. This represents an existing grid where no measures have been taken to enable hosting LCTs. There are no investment costs and the life-cycle cost for this initial grid is composed only of operating costs to cover energy losses (see Section 2.3). We consider the following grid modifications that allow hosting the new LCTs by alleviating potential voltage and loading problems at the level of the transformer and of the detailed feeder:

- Replacement of the distribution transformer by one with higher nominal capacity.
- Replacement of the main cables of the detailed feeder (3 phases and neutral) by cables of larger cross-section, and thus larger current carrying capacity. In this article, for the sake of simplicity and to cover extreme cases, we refer to whole feeder upgrade but it is also possible to replace only parts of the feeder. However, that would require simulation of many more reinforcement options that reflect partial replacement of the feeder cables. Nevertheless, the overall methodology would not be modified by this choice, the only differences being that different cross-sections would be encountered along

the detailed feeder and that the feeder replacement cost would be proportional to the share of the feeder replaced (see second term in equation (7)).

- Connection of the LCTs in dwellings of the detailed feeder to three phases instead of one.

A reinforcement option can be composed of one of the three above-mentioned modifications, or any combinations between these modifications (e.g. replacing both the transformer and the feeder cables).

2.1.3 Techno-economic evaluation of a grid reinforcement option for a low-carbon technology integration scenario

Each LCT integration scenario and grid reinforcement option is evaluated thanks to the technical and economic models as shown in Figure 2. The technical model simulates the influence of an LCT integration scenario and a grid reinforcement option on four grid stability indicators, as described in Section 2.2. The economic model computes the life-cycle cost per dwelling LCC_d associated to a grid reinforcement option (see Section 2.3).

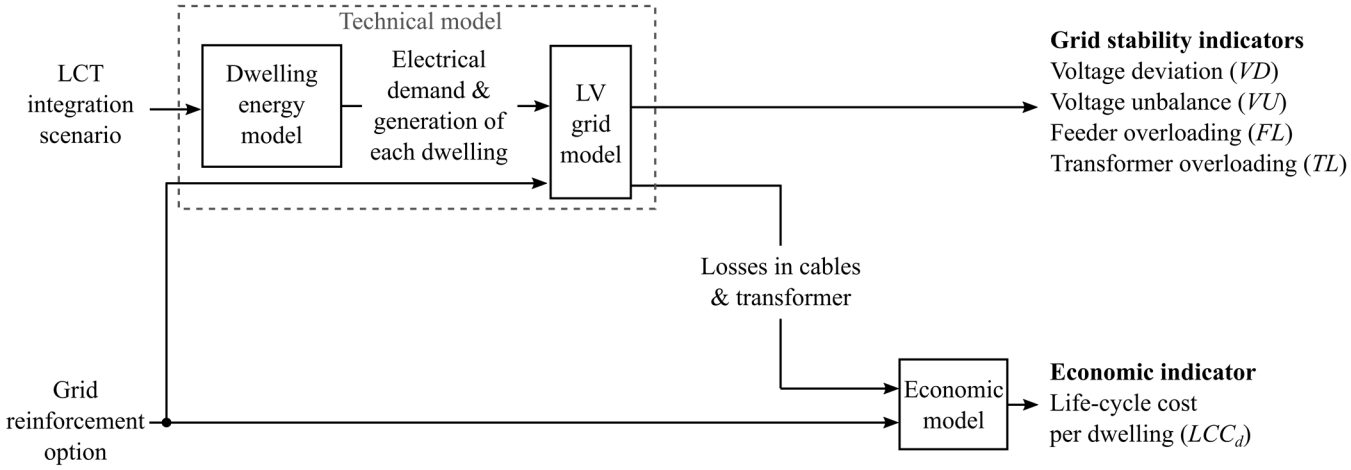

Figure 2 – Evaluation of LCT integration scenarios and grid reinforcement options.

In order to capture uncertainties in demand and generation, as well as the random distribution of LCTs in a feeder, the methodology offers the possibility to perform several repetitions for each LCT integration scenario [35]. For each scenario and repetition, random dwellings and occupants are sampled from an available pool, and the locations of the LCTs on the feeder are also randomly selected. The technical and economic models are then evaluated for all reinforcement options for this repetition and scenario. A reinforcement option is considered technically viable for a given LCT integration scenario when all four grid stability indicators are within the required limits for all performed repetitions (see Section 2.2.3) and its associated cost is calculated as the average among all repetitions (see Section 2.3). The cost of the cheapest technically viable reinforcement option is finally chosen as reinforcement cost for the LCT integration scenario. The same procedure is followed for all scenarios. The number of repetitions should be chosen depending on the desired robustness and the available computing time for the considered case study (see Section 3.2.3).

The methodology can be used on typical grids for a region or country, in order to provide an estimate of the reinforcement costs per dwelling (see Section 3). Furthermore, the same models and approach can also be used to perform analysis on a specific real feeder. The rest of the island to which the feeder belongs would then be represented as an aggregated load. In this case, random repetitions may not be required as the properties of the dwellings, occupants and LCTs may be known.

2.2 Technical model

As show in Figure 2, the technical model is composed of two sub-models: the dwelling energy model and the LV grid model. Both are implemented using the Modelica IDEAS library and simulated with the Dymola software. Modelica is a non-proprietary, domain-neutral, object-oriented language that provides flexibility for continuous development. The IDEAS library was specifically created to integrate dynamic simulation of electrical and thermal systems at district level. It has been presented in [36] and is available at https://github.com/open-ideas. In this section, we first present the dwelling energy model that is used to generate a pool of electrical demand and generation profiles that correspond to dwellings with the desired integrated LCTs (Section 2.2.1). The pool of profiles is then used to draw inputs for the LV grid model, which is based on power flow analysis (Section 2.2.2). Finally we detail the outputs of the technical model (see Figure 2): the defined grid stability indicators (Section 2.2.3), and the energy losses in the cables and in the transformer (Section 2.2.4), which are inputs to the economic model.

2.2.1 Dwelling energy model

In the following, we summarize the dwelling energy model which is detailed in [31]. This model currently integrates HPs and PV systems as LCTs, but given its modular structure and customizable components, it is also possible to integrate other LCTs, such as electric vehicles, in the future. In any case, different sources may be used in the overall methodology presented in Figure 2 to provide the necessary pool of electrical demand and generation profiles.

Our dwelling energy model is composed of three main components as shown in Figure 3, namely the occupancy model, the building model and the PV model. Figure 3 also shows where LCT integration has an influence. A pool of dwellings is created by sampling dwelling properties from predefined probability distributions. Each dwelling is assigned a set of occupant profiles, providing the necessary boundary conditions. The thermal building model then simulates the thermal and electrical demand for the given building properties, occupants, heating system (e.g. heat pump), and weather conditions. Furthermore, PV generation is simulated for the same weather and for variable installation sizes in accordance with the dwelling properties. The individual components of the model are presented below in more detail.

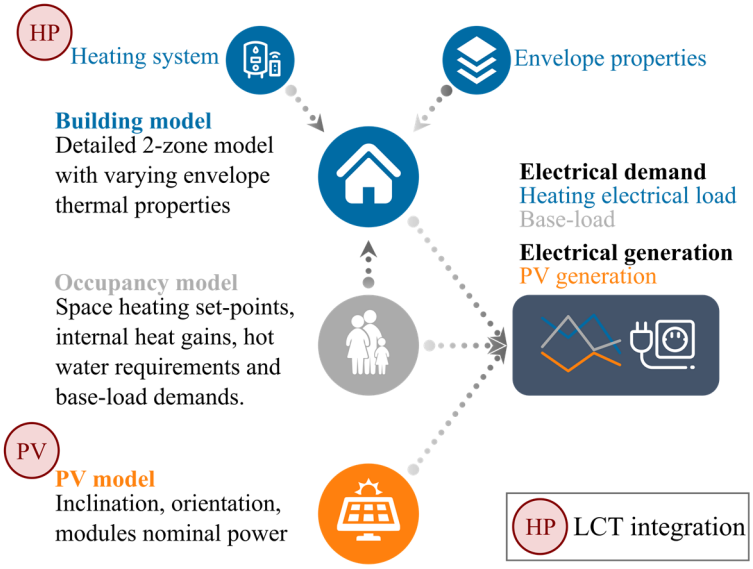

Figure 3 – Main components of the dwelling energy model.

Occupancy model. The stochastic residential occupancy model consists in the Python StROBe Package as presented in [37]. The model generates sets of profiles that include what we refer to as "base load", representing active power demand profiles for lighting, large and small domestic appliances and electronics (e.g. fridge, washing machine, television). The occupant model also provides space-heating set-points, internal heat gains and hot-water demand, which are inputs to the building model.

Building model. The building model computes the electrical heat demand from the outputs of the occupancy model, the properties of the building envelope and the chosen heating system. The first step is to quantify the thermal heat demand, which includes the space heating and domestic hot water demands. The thermal heat demand is obtained by a detailed thermal building model based on the envelope properties, using inputs from the occupancy model and the weather data (in particular outdoor temperature and irradiance). The main envelope properties are the floor area, window-to-wall ratio, orientation, general envelope thermal quality and infiltration rate, most of which highly depend on the dwelling type (detached, semi-detached or terraced). These properties are either known for the considered LV island, or they can be generated by using representative data of the building stock in the studied area (see Section 3.1). The thermal demand can be met by electricity (e.g. HP which are the focus of this work) or by other energy sources (e.g. gas boiler). We consider air-source HPs rather than ground-source HPs, as they are the most common ones [38] [39] and are also expected to have a higher impact on the grid [3]. The HP is considered to provide hot water to low-temperature radiators in each thermal zone and to a domestic hot water storage tank. The HP model is based on interpolation in a performance map retrieved from manufacturer data [40] [41], which defines the heating power and electricity use (active power) as function of the heating requirements. Back-up instantaneous electric heaters of a few kW are also usually installed to assists the HP in space heating in very cold days and to support water heating when the HP is not sufficient and for anti-legionella heating cycles in the water storage tank.

PV model. High-resolution PV generation profiles are also needed for the analysis. A 10-minute temporal resolution for the PV profiles is a good compromise between the temporal resolution required to compute grid stability indicators (see Section 2.2.3) and simulation time. Here, a PV model based on the 5-parameter model of De Soto [42] is used to generate active power PV production

profiles from the weather data (irradiance and outdoor temperature) for the specific orientation, inclination and nominal capacity of each dwelling's PV system. In the feeder simulation, for each dwelling with a PV system the electricity produced is first used to cover the dwelling's demand and the rest is injected to the feeder. To avoid potential excessive feeder voltages, the PV system inverter can be disconnected when voltage at the dwelling's switchboard reaches a given limit.

Furthermore, since all load and generation profiles include only active power, we also implement a power factor for each profile, which determines the equivalent reactive power profile.

Figure 4 presents an example of load and generation profiles obtained from the dwelling energy model for one dwelling during three days with a time step of 10 minutes. It corresponds to the case of a detached Belgian house (average envelope U-value: 0.64 W/m^{2}K).

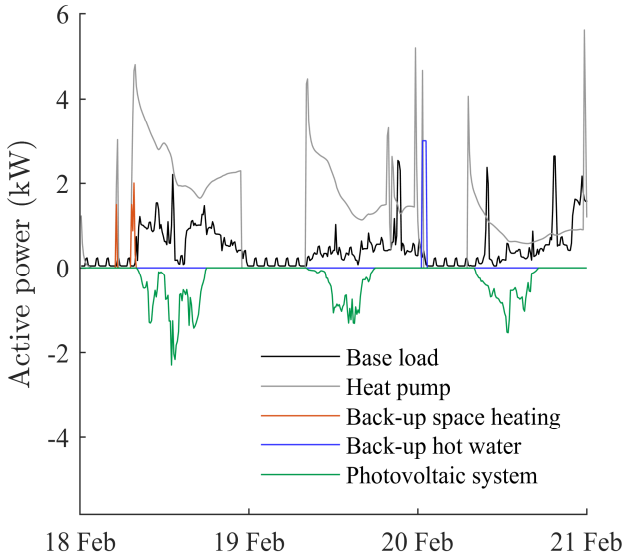

Figure 4 – Example of dwelling's load and generation profiles produced by the dwelling energy model.

2.2.2 Low-voltage grid model

The used grid architecture for the considered grids was presented in Figure 1. The LV distribution island consists in a medium voltage/low voltage (MV/LV) transformer, a detailed feeder and a dummy feeder representing the loads in the rest of the island. The distribution network is a single-point grounded network, where the grounding is defined at the MV/LV transformer. The voltage on the MV side of the transformer and the transformer transformation ratio are considered constant. When single-phase connections are examined, the dwelling connections are alternating between the three phases, as depicted in Figure 1. The grid model and quasi-stationary power flow analysis are implemented in Modelica, using components of the IDEAS library [43]. The model receives as input the active and reactive power profiles of each dwelling, which are applied at each connection point in the detailed feeder, or aggregated and applied as a balanced load in a dummy feeder for the rest of the island. The power flow analysis is based on Kirchhoff's circuit laws and Joule's law [43], which determines for each simulation time step the current and voltage at all branches and nodes. For this analysis, we specifically define the following outputs:

- The line-to-neutral voltage at each dwelling connection of the detailed feeder. We denote $v(dc_k^j)$ the line-to-neutral voltage at dwelling connection dc_k^j, corresponding to the connection of the dwelling in position k to phase j (see Figure 1). If the dwelling is connected to 3 phases, 3 dwelling connections are defined.
- The line-to-line voltages at each node of the detailed feeder. The line-to-line voltage at the node in position k between phases j and j' is denoted $v(n_k^{j,j'})$. In order to be able to calculate voltage unbalance (see Section 2.2.3), the line-to-line voltages between all three phases are defined for all positions k even for positions where the dwelling is connected to only one phase. For instance, in Figure 1, $v(n_4^{1,2})$, $v(n_4^{2,3})$ and $v(n_4^{3,1})$ are defined for node 4, even though the dwelling is connected only to phase 1 at this position.
- The current in each feeder segment of the detailed feeder $i(fs)$.
- The current in each dwelling link connected to the detailed feeder $i(dl)$.
- The apparent power through the transformer $S(\tau)$.
- The current in each phase j of the transformer $i(\tau^j)$.

2.2.3 Grid stability indicators

We propose grid stability indicators based on the outputs of the LV grid model. The indicators were defined not only to know when a grid stability constraint is violated, but also to represent the magnitude of this violation. Out of four grid stability indicators detailed in the following paragraphs, the voltage deviation, voltage unbalance and feeder overloading indicators are computed for the detailed feeder, and the transformer overloading is computed for the transformer serving the entire distribution island (see Figure 1).

Voltage deviation indicator VD. The voltage at each dwelling connection $v\left(dc_k^j\right)$ is subject to the limitations imposed by European Standard EN 50160 [44] [45]. It requires the per unit voltage (expressed as fraction of the nominal voltage, 230 V in Europe) to remain between 0.9 and 1.1 pu for more than 95 percent of the time each week, and never below 0.85 or above 1.1 pu [44] [45]. The voltage levels should be evaluated every 10 minutes [44], so if the initial voltage profile is obtained with a resolution finer than 10 minutes, a 10-min moving average filter should be first applied. To check compliance with the Standard, we define the voltage deviation indicator for dwelling d_k: $VD(d_k)$. If the dwelling is connected to one phase only, $VD(d_k)$ is equal to 1 if the Standard on voltage deviation is violated at least once during the whole simulation period for the phase to which the dwelling is connected, and equal to 0 otherwise. If at least one of the appliances (e.g. HP, PV) in the dwelling is connected to three phases, $VD(d_k)$ is equal to 1 if the Standard on voltage deviation is violated at least once during the whole simulation period for any of the three phases, and to 0 otherwise. The voltage deviation indicator for the whole feeder VD is the sum of the $VD(d_k)$ divided by the number of dwellings in the feeder D_f. VD thus represents the share of dwellings for which there are voltage deviation problems. If VD is higher than 0, the simulated case is considered technically unsustainable.

Voltage unbalance indicator VU. We define the voltage unbalance at the node n_k in position k at time t, using the formula proposed by [46]:

$$vu(n_k)(t) = \sqrt{\frac{1-\sqrt{3-6\cdot\beta(t)}}{1+\sqrt{3-6\cdot\beta(t)}}} \quad \text{where} \quad \beta(t) = \frac{\left(v\left(n_k^{1,2}\right)(t)\right)^4 + \left(v\left(n_k^{2,3}\right)(t)\right)^4 + \left(v\left(n_k^{3,1}\right)(t)\right)^4}{\left(\left(v\left(n_k^{1,2}\right)(t)\right)^2 + \left(v\left(n_k^{2,3}\right)(t)\right)^2 + \left(v\left(n_k^{3,1}\right)(t)\right)^2\right)^2} \tag{1}$$

The voltage unbalance should also be evaluated with a time step of 10 minutes [44]. The European Standard EN 50160 subjects the voltage unbalance at each node to remain below 2% for more than 95% of the time each week [30] [44]. We thus define the voltage unbalance indicator at node n_k: $VU(n_k)$, which is equal to 1 if the Standard on voltage unbalance is violated at least once during the whole simulation period, and to 0 otherwise. The voltage unbalance indicator for the whole feeder VU is the sum of the $VU(n_k)$ divided by the number of nodes in the feeder. VU thus represents the share of nodes for which there are voltage unbalance problems. If VU is higher than 0, the simulated case is considered technically unsustainable.

Feeder overloading indicator FL. We define the overloading of feeder segment fs at time t as [45]:

$$fl(fs)(t) = \max\left(\frac{|i_h(fs)(t)|}{i_{nom}(fs)} - 1, 0\right) \tag{2}$$

where $i_h(fs)$ is the hourly average current in the feeder segment and $i_{nom}(fs)$ is the current carrying capacity of the feeder segment. $fl(fs)$ is thus computed with a time step of 60 min [45]. We further define the feeder overloading indicator of the feeder segment: $FL(fs)$. This indicator is equal to 1 if $fl(fs)$ is higher than 0, i.e. the cable segment is overloaded [45], at least once during the whole simulation period, and to 0 otherwise. The feeder overloading indicator for the whole feeder FL is the length-weighted mean of the $FL(fs)$. FL thus represents the share of the total feeder segment length for which there are overloading problems. If FL is higher than 0, the simulated case is considered technically unsustainable.

Transformer overloading TL. We define the overloading of the transformer τ at time t as [45]:

$$tl(\tau)(t) = \max\left(\frac{|S_h(\tau)(t)|}{S_{nom}(\tau)} - 1, 0\right) \tag{3}$$

where $S_h(\tau)$ is the hourly average apparent power that goes through the transformer τ and $S_{nom}(\tau)$ is the nominal capacity of the transformer. The transformer overloading $tl(\tau)$ is thus defined with a time step of 60 min. The transformer overloading indicator TL is the maximum of the transformer overloading $tl(\tau)$ during the simulation period. If TL is higher than 0, the transformer is overloaded [45], and the simulated case is considered technically unsustainable.

The above definitions were formulated for one repetition. When several repetitions are used, then each indicator is averaged among all repetitions. Thus, a reinforcement option for a given scenario is considered viable only if the indicators of all repetitions are equal to 0.

Note that, even though the voltage deviation and unbalance indicators are defined based on the requirements of the European norm in this article, similar indicators representing the same grid stability issues can be defined for norms of other countries using the same input signals (voltages at the dwelling connections and at the nodes).

2.2.4 Losses in cables and transformer

The technical model also allows computing the yearly energy losses in the transformer $E_l(\tau)$ and in the detailed feeder $E_l(f)$, which are inputs to the economic model (see Figure 2).

The energy losses in the transformer $E_l(\tau)$ for year y are given by [33]:

$$E_l(\tau)(y) = \int_y \left(P_0(\tau) + \sum_{j=1}^{3} R(\tau^j) \left| i(\tau^j)(t) \right|^2 \right) dt \tag{4}$$

where $P_0(\tau)$ are the transformer no-load losses, $i(\tau^j)$ is the current through phase j of the transformer and $R(\tau^j)$ is the phase resistance of the transformer (which is considered identical for the three phases [33]). Given that the voltage at the transformer level remains close to 1 pu, the dependence of the transformer no-load losses on voltage is not considered in this article.

The energy losses in the detailed feeder $E_l(f)$ for year y are obtained from the joule losses in each feeder section fs (which includes the three phases and the neutral, see Figure 1) and dwelling link dl. $E_l(f)$ is given by [33]:

$$E_l(f)(y) = \int_y \left(\sum_{fs} R_l(fs) \cdot l(fs) \cdot |i(fs)(t)|^2 + \sum_{dl} R_l(dl) \cdot l(dl) \cdot |i(dl)(t)|^2 \right) dt \tag{5}$$

where $R_l(fs)$ and $R_l(dl)$ are the linear resistances of the feeder segment fs and the dwelling link dl respectively, and $l(fs)$ and $l(dl)$ are their lengths. Note that, as we consider unbalanced power flow, there may be losses in the neutral conductor.

2.3 Economic model

We compute the life-cycle cost associated to reinforcements of the detailed feeder. It accounts for the investment cost IC and the operating costs OC during the considered lifetime L (i.e. the planning horizon for grid reinforcements). The cost for the detailed feeder is then divided by the number of dwellings in this feeder D_f in order to be able to compare costs between grids with different number of dwellings. The life-cycle cost per dwelling LCC_d is given by [47] [48]:

$$LCC_d = \frac{IC + \sum_{y=1}^{L} \frac{OC(y)}{(1+\delta)^y}}{D_f} \tag{6}$$

where δ is the discount rate. This cost is computed for one repetition. When several repetitions are used, we consider the average cost between all repetitions.

2.3.1 Investment cost

The investment cost IC for the feeder is given by [30] [49]:

$$IC = b_\tau \cdot C(\tau) \cdot \frac{D_f}{D_i} + b_f \left(l_t(f) \cdot C_l(f) + D_f \cdot C_r \right) + \sum_{d=1}^{D_f} b_{3\phi}(d) \left(C_{3\phi,m} + l(dl) \cdot C_l(dl) + \bar{b_f} \cdot C_r \right) \tag{7}$$

$b_\tau \cdot C(\tau) \cdot \frac{D_f}{D_i}$ is the cost related to the replacement of the transformer by one with a higher nominal capacity. b_τ is a binary variable which is equal to 1 if the transformer is replaced, $C(\tau)$ is the cost of replacing the existing transformer by a new transformer τ, D_f and D_i are the number of dwellings in the feeder and in the island respectively. The ratio D_f/D_i represents the share of the transformer replacement cost that is attributable to the detailed feeder.

$b_f \left(l_t(f) \cdot C_l(f) + D_f \cdot C_r \right)$ is the cost related to the replacement of the main cables of the detailed feeder by cables of higher cross-section. b_f is a binary variable which is equal to 1 if the cables are replaced, $l_t(f)$ is the length of the detailed feeder (see Figure 1), $C_l(f)$ is the linear cost of replacing the existing feeder cables by new ones and C_r is the cost of reconnecting a dwelling link to the feeder.

$\sum_{d=1}^{D_f} b_{3\phi}(d)\left(C_{3\phi,m} + l(dl) \cdot C_l(dl) + \overline{b_f} \cdot C_r\right)$ is the cost associated to connecting LCTs of dwellings of the detailed feeder to three phases. It is assumed that buildings are originally connected to a single phase, and therefore a new link is required in this case. $b_{3\phi}(d)$ is a binary variable which is equal to 1 if the dwelling has at least one LCT connected to three phases, $C_{3\phi,m}$ is the cost of a three-phase meter, $l(dl)$ is the length of the dwelling link, $C_l(dl)$ is the linear cost of replacing the current one-phase dwelling link by a three-phase cable. $\overline{b_f}$ is the negation of the b_f binary variable, used to include the cost of reconnecting dwelling links to the feeder, only if the main feeder cables are themselves not replaced. In the latter case, this cost is already accounted for in the feeder replacement cost.

2.3.2 Operating costs

The operating costs are related to energy losses in the transformer τ and feeder f. The annual operating cost OC for year y is given by [30] [50]:

$$OC(y) = \left(E_l(\tau)(y) \cdot \frac{D_f}{D_i} + E_l(f)(y)\right) \cdot C(E_l) \tag{8}$$

where $C(E_l)$ is the cost per kWh of energy losses for the DSO.

3 Integration of heat pumps and photovoltaic systems in Belgian low-voltage grids

In this section, we apply the proposed methodology to investigate the adapted reinforcements to the integration of HPs and PV systems in typical Belgian rural and urban LV grids. The study parameters are presented in Section 3.1 and the results in Section 3.2.

3.1 Study parameters

The study parameters and their supporting references are summarized in Table 1 and commented in the paragraphs below. The grid and dwelling parameters and the economic parameters were mostly determined from our previous studies on Belgian feeders [30] [31] [33] [51] and cost data of the Belgian DSO Fluvius [30] [49].

Table 1 - Summary of the parameters for the Belgian rural and urban cases.

Grid and building parameters		
	Rural	*Urban*
Number of dwellings in the detailed feeder D_f	15 [30]	15 [30]
Number of dwellings in island D_i	73 [31]	108 [31]
Average length between feeder nodes $l_a(f)$	22 m [31]	7 m [31]
Total length of the detailed feeder $l_t(f)$	330 m	105 m
Length of dwelling links $l(dl)$	8 m [31]	3 m [31]
Cross-section of dwelling links	16 mm² [33]	16 mm² [33]
Building types	4% terraced, 20% semi-detached, 76% detached [31]. Buildings randomly chosen from a building stock (average envelope U-value of buildings between 0.25 and 0.80 W/m²K) [31].	80% terraced, 20% semi-detached [31]. Buildings randomly chosen from a building stock (average envelope U-value of buildings between 0.25 and 0.80 W/m²K) [31].
Power factors	Base loads: 0.98 [45], HP: 0.98 [31] [45], PV: 1 [52] [53]	
LCT integration scenarios		
HP integration rates	[0, 20, 40, 60, 80, 100] % [51]	
PV integration rates	[0, 20, 40, 60, 80, 100] % [51]	
Reinforcement options		
Transformer nominal power $S_{nom}(\tau)$	No reinforcement: 160 kVA [30] Reinforcement: 250, 400 kVA [30]	
Cross-section of main feeder cables	No reinforcement: 70 mm² (current carrying capacity i_{nom} of 225 A) [30] [31] [35] Reinforcement: 150 mm² (current carrying capacity i_{nom} of 315 A) [30] [31] [35]	
Number of phases to which HPs are connected	No reinforcement: 1 Reinforcement: 3	
Number of phases to which PV systems are connected	No reinforcement: 1 Reinforcement: 3	
Economic inputs		
Planning horizon L	33 years [54].	
Discount rate δ	5% [48]	
Transformer replacement cost $C(\tau)$	160 kVA (capacity of the newly installed transformer τ) : $C(\tau)$ = 6365 € [30]* 250 kVA : $C(\tau)$ = 7969 € [30]* 400 kVA : $C(\tau)$ = 10973 € [30]*	
Main feeder cables replacement linear cost $C_l(f)$	39 €/m (rural), 52 €/m (urban) [30]*	
Cost of reconnecting a dwelling link to the feeder C_r	486 € [30]*	
Cost of a 3-phase meter $C_{3\phi,m}$	149 € [49]	
Dwelling link replacement linear cost $C_l(dl)$	Same as $C_l(f)$ [30]*	
Energy losses cost $C(E_l)$	0.046 €/kWh [55]	
Simulation parameters		
Simulation time step	10 minutes [31]	
Simulation time and weather data	1 year of extreme weather data (low temperature in winter and high irradiance in summer) [31] [56]	

Notes

The value-added tax is not included in the costs [30].

*: Costs that were obtained for years earlier than 2020. They have been corrected for inflation using a 1.5% yearly rate [57] to transpose to the year of study. The values given in the table for these costs are therefore "2020 equivalent" ones.

Grid and building parameters. Figure 5 presents the typical rural and urban LV grids considered. The number of dwellings in the

detailed feeder is the same for the rural and the urban grid but the whole island is larger in the case of the urban grid. The average distance between nodes is three times higher in the rural feeder than in the urban one. The customer density is of ~5 dwellings per 100 m for the rural grid and of ~14 dwellings per 100 m for the urban one. For both feeder types, the nodes are equally spaced except for an exceptional random length, which is several times the usual length between nodes. This exceptional length is positioned at the beginning of the urban feeder and in the middle of the rural one, to represent exceptional distances encountered in real feeders [31]. The dwelling links are also longer for the rural feeder than for the urban one and we consider 16 mm^2 cables for these links. We verified that the dwelling links are never overloaded in all of the simulated cases.

Detached dwellings make the majority of the rural island, while the urban island is mostly composed of terraced dwellings, with some semi-detached dwellings mostly at the ends of urban feeders, as would be in a real street. Given these guidelines, the type (terraced, semi-detached, detached) of each dwelling is randomly chosen. The buildings are randomly sampled from a building stock of 300 different buildings, which was created using an optimised Latin Hypercube design based on typical ranges of the building properties corresponding to Belgian houses [31]. For both the urban and the rural feeder, we sample a random mix of old and renovated dwellings out of the building stock, which corresponds to average envelope U-values between 0.25 and 0.80 W/m²K. Each dwelling also has a 200 L domestic hot water storage tank [51]. Furthermore, each dwelling is allocated a random set of occupant profiles [37].

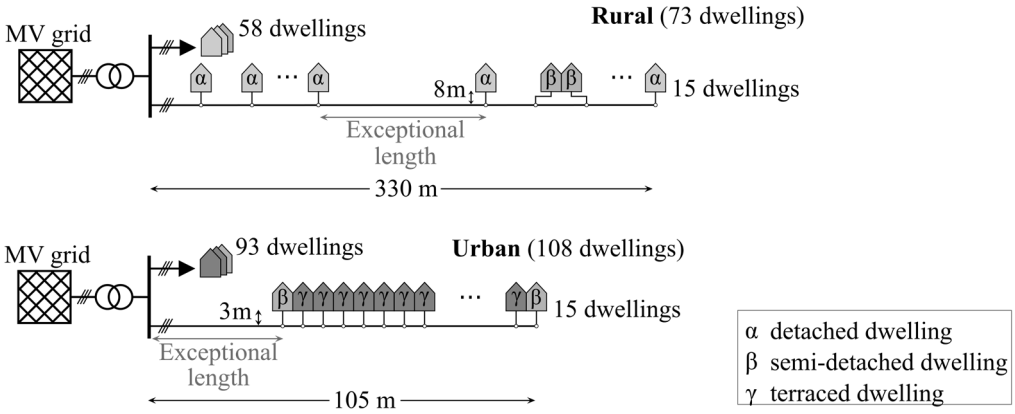

Figure 5 – Typical rural and urban LV grids considered.
The three phases of the detailed feeder are not shown in this figure.

LCT integration scenarios. We consider all possible combinations of HP and PV integration rates between 0 and 100% with a step of 20%. The dwellings that receive a HP and/or a PV system are randomly and independently selected. When the dwelling is not equipped with a HP, we consider that the thermal heat demand is met by a gas boiler [51] and therefore that there is no electrical heat demand. For each dwelling with HP, the HP is sized based on the design heat load, as defined by Standard NBN EN 12831 [58]. The resulting maximum heat pump electric power among all buildings varies between 1.1 and 8.5 kW. Back-up electric elements for space and hot water are considered, with a capacity of 3 kW each. For each dwelling with PV system, the PV panels are inclined of 34° and their orientation is either south, west or east depending on the building orientation [31] [51]. Their nominal power is randomly selected between 3 and 5 kW, also taking into account the roof's dimensions (we consider that no more than 80% of the roof area on one façade can be covered by PV panels) [31]. Regarding PV curtailment, we consider that the PV system inverter is disconnected for a minimum duration of 10 minutes, when voltage at the dwelling's switchboard reaches 1.1 pu (i.e. 253 V for a nominal voltage of 230 V) [31].

Reinforcement options. When there are no reinforcements (initial grid), we consider a 160 kVA transformer and main feeder cables of cross-section 70 mm^2. All grid stability indicators are equal to 0 for a 0% integration of HP and PV in this initial grid, meaning that it is a technically viable option when only the base loads are served. As LCT integration levels are increased, the HPs and PV systems are connected by default to the same phase as all other loads of the building.

Grid reinforcement options consist in any combination of transformer replacement, feeder replacement and three-phase connection of the LCTs. The transformer may be replaced by a 250 kVA or 400 kVA one, the main feeder cables by cables of cross-section 150 mm^2, and all HPs and/or PV systems can be connected to three phases instead of one. We consider that either all or none of the LCTs of the same type are connected to three phases (e.g. all PV systems connected to 3 phases), limiting the number of grid reinforcement options considered. This allows to keep the simulation time reasonable and to favour the clarity of the results, while covering the largest range of possibilities. An example of reinforcement option would be replacing the 160 kVA transformer by a 250 kVA one, maintaining the initial main feeder cables, connecting all HPs to three phases, and connecting all PV systems to one phase.

Economic inputs. Regarding the replacement of the main feeder cables and of the dwelling links (the latter occurs when LCTs are connected to three phases), we consider that current cables (which may have been overhead or underground) are replaced by underground ones, as underground cables are now strongly encouraged in Belgium [30]. The linear cost of replacing a cable is driven by labour costs for opening and closing the trench where the new cable is placed [13] [30]. Consequently, this linear cost can be assumed to remain the same for the main feeder cables and dwelling links, regardless of whether they had been overhead or underground [30]. However, this cost depends on the ground type, which explains why it is higher in urban areas, where we consider 100% 'sidewalk' type ground, than in rural ones, where we consider 50% 'sidewalk' type ground and 50% 'meadow' type ground (see reference [30] for the costs of replacing cables below 'sidewalk' and 'meadow' type grounds). Regarding the cost of energy losses $C(E_l)$, we can consider that, in Belgium, the DSO commits to pay for them at a given price for the following years (obtained from reference [55]). For instance if the contract is settled in January 2020, the DSO will have to pay 0.044 €/kWh for 2021, 0.046 €/kWh for 2022 and 0.047 €/kWh for 2023 (which is the furthest year currently available). We choose the average between these three values 0.046 €/kWh as the value of $C(E_l)$ for our study.

Simulation parameters. The technical model, including occupant profiles, the building models and power flow are simulated for one year with a time step of 10 min [30] [31]. Consequently, the operating cost $OC(y)$ is the same for each year y of the planning horizon L (33 years). We use weather data, provided by the Meteonorm [56], for Uccle (Belgium) representative of an extreme year for the considered case study: low temperature in winter (and therefore high HP electrical demand) and high irradiance in summer (and therefore high PV generation). Indeed, such an extreme year may occur during the planning horizon, and the DSO may want to use it for its analysis in order to be on the conservative side.

In total, for each typical grid (rural, urban), there are 36 LCT integration scenarios (all combinations of HP and PV integration rates). Furthermore, for each integration scenario, the initial grid as well as all possible reinforcement options are investigated, namely a maximum of 24 cases for scenarios with both HP and PV integration. Last, for most assessed indicators several repetitions are evaluated, each corresponding to different random sampling of dwellings and the location of LCTs. For a given typical grid (rural/urban), 726 simulations are performed in total per repetition. Evaluating all these 726 simulations takes ~5 hours using a Precision 7910 Tower (Dual Intel Xeon E5-2640 v4 2.4 GHz processors, 128 GB RAM, running on Windows 10 Pro 64-bit) [59] and with 24 simulations running in parallel.

3.2 Results

The results regarding the influence of LCT integration on the grid stability and reinforcement cost (see Sections 3.2.1 and 3.2.2) are obtained for 68 random repetitions for the rural grid and 27 random repetitions for the urban grid. This choice of the number of random repetitions is justified in Section 3.2.3, where we investigate the influence of the number of repetitions on the results. In terms of computing time, it took 14 days to obtain the results for the rural grid and 6 days to obtain the results for the urban grid.

3.2.1 Influence of low-carbon technologies integration and reinforcements on grid stability

In this section, we detail and analyse the influence of separate integration of LCTs and of reinforcement options on grid stability indicators and the reinforcement cost LCC_d (combined LCT integration is considered in section 3.2.2). The presented results also allow evaluating the suitability of grid reinforcement options for different levels of LCT integration and identifying which options may become unviable once a given level of integration is reached.

Rural grid

For the rural grid, Table 2 presents the influence of increasing HP integration on the grid stability indicators and on the LCC_d for all reinforcement options and for a PV rate of 0%. There are only 12 reinforcement options in this case, as there are no PV systems (which thus cannot be connected to 1 or 3 phases). The results of Table 2 are obtained for 68 repetitions, meaning that, for each integration rate and reinforcement option, the value given for each indicator (e.g. VD) is obtained by averaging the values of this indicator for the 68 repetitions performed. In Table 2, for each HP integration rate, we also highlight in green the cost of the cheapest technically viable reinforcement option, denoted as LCC_d^*. It corresponds to the option for which all technical indicators are equal to 0 (i.e. option viable in view of all indicators and for all 68 repetitions) and for which the cost is the lowest.

Table 2 – Influence of the HP integration rate and of the choice or reinforcement option on the grid stability indicators and the LCC_d. Rural grid, PV integration rate fixed at 0%, 68 random repetitions.

%HP		τ_1, f_1, ϕ_1	τ_1, f_1, ϕ_3	τ_1, f_2, ϕ_1	τ_1, f_2, ϕ_3	τ_2, f_1, ϕ_1	τ_2, f_1, ϕ_3	τ_2, f_2, ϕ_1	τ_2, f_2, ϕ_3	τ_3, f_1, ϕ_1	τ_3, f_1, ϕ_3	τ_3, f_2, ϕ_1	τ_3, f_2, ϕ_3
0%	VD												
	VU												
	FL												
	TL												
	LCC_d (€)	49		1386		162		1499		213		1551	
20%	VD												
	VU												
	FL												
	TL												
	LCC_d (€)	63	247	1396	1485	174	358	1507	1597	224	408	1557	1646
40%	VD	0.02				0.01				0.01			
	VU	0.01				0.01							
	FL												
	TL	0.01											
	LCC_d (€)	84	451	1411	1589	192	559	1519	1697	239	607	1566	1745
60%	VD	0.1				0.02				0.01			
	VU	0.03				0.01							
	FL												
	TL	0.2	0.2	0.2	0.19								
	LCC_d (€)	107	659	1428	1696	210	762	1531	1799	254	807	1576	1844
80%	VD	0.25	0.01	0.01		0.07				0.02			
	VU	0.07				0.01							
	FL												
	TL	0.48	0.48	0.48	0.48	0.01	0.01	0.01	0.01				
	LCC_d (€)	134	871	1448	1805	231	969	1545	1903	271	1010	1587	1944
100%	VD	0.51	0.41	0.05		0.13				0.03			
	VU	0.06											
	FL												
	TL	0.8	0.8	0.79	0.79	0.15	0.15	0.15	0.15				
	LCC_d (€)	165	1088	1471	1919	254	1179	1562	2010	290	1215	1599	2047

Notes

τ_1, τ_2, τ_3: are the 160, 250 and 400 kVA transformers respectively; f_1, f_2: are the 70 mm^2 and 150 mm^2 main feeder cables respectively; ϕ_1, ϕ_3: correspond to the one and three phase connection of heat pumps.

Only non-zero values are presented. Values of grid stability indicators strictly larger than 0 and smaller than 0.01 are rounded up to 0.01.

For 0% HP, the distinction between reinforcement options associated to the connection of HPs to one or three phases does not make sense. Thus the results for ϕ_1 and ϕ_3 are merged.

For each HP integration rate, the cost of the cheapest technically viable reinforcement option is highlighted in green.

Comparison of the LCC_d of the initial grid (first column in Table 2) with that of other reinforcement options reveals that grid reinforcements may lead to more significant costs than energy losses, which represent the only cost in the initial grid. For the cases presented in Table 2, when looking at the breakdown of the overall cost LCC_d between energy losses and investments in reinforcements (not shown in Table 2), we observed that the cost of energy losses over the lifetime ranges from 42 to 165 € per dwelling, while the investment cost for reinforcements ranges from 0 to 1955 € per dwelling. Looking into the cost per reinforcement category, transformer replacement (~100-150 €/dwelling) is cheaper than switching to three phase connection (~200-950 €/dwelling) which is itself cheaper than feeder replacement (~1350 €/dwelling). This overall trend is also observed in the cases with other PV integration rates and in urban grids.

Concerning grid stability indicators, we observe in Table 2 that all the indicators are equal to 0 for 0% and 20% HP. In these cases, no investments are thus required for reinforcements and the life-cycle cost of the cheapest technically viable option LCC_d^* (highlighted in green in Table 2) only corresponds to operating costs to cover energy losses. Moreover, results in Table 2 indicate

that the feeder is never overloaded ($FL = 0$) and that transformer loading is gradually affected by HP integration, which thus requires transformer replacement. HP integration also affects voltage unbalance and to a greater extent voltage deviation, in which case voltage deviation corresponds to under voltages. Transformer replacement allows decreasing voltage deviation and unbalance problems, as it reduces voltage variation, but it does not completely restore voltage stability. Thus, either feeder replacement or three-phase connection of the HPs is required. In terms of cost, three-phase connection is cheaper than feeder replacement, and it is thus preferred. This result is in line with the recent requirement of the Belgian DSO Fluvius to connect HPs of more than 5 kW electric capacity to three phases [60].

The influence of PV integration (for a 0% HP integration rate) on the grid stability indicators and the LCC_d was also studied. In this case, there were no violations of the voltage constraints, and no feeder overloading for any PV integration rate. The only grid stability indicator that is affected by PV integration is transformer overloading TL, due to the excessive power flow from PV systems in the LV grid to the MV grid during very sunny days. More specifically, the 160 kVA transformer has to be replaced by a 250 kVA one for a PV integration of 80% and 100% (for lower PV integration rates, no reinforcements are required and the cost LCC_d^* is only due to energy losses). This would suggest that, for the examined grid, no major reinforcements would be needed due to the sole integration of PV, contrarily to HP integration. This is especially because HP power consumption adds up to the base load, while PV generation is subtracted from it (see Figure 4).

Urban grid

Regarding the urban grid, results indicate that HP and PV integration does not cause voltage violations or feeder overloading. The lack of voltage violations from HP integration in the urban grid, contrary to the rural grid, is due to two main reasons. First, the shorter feeder length between two consecutive dwellings (linked to higher customer density) in the urban case leads to smaller voltage drops, reducing both voltage deviation problems and unbalance between the phases. Second, electric power consumption of heat pumps in urban grids is on average lower than in rural grids. Indeed, the predominantly terraced dwellings are smaller and have less heat losses to the environment than dwellings of the rural grid, which are mostly detached. The only grid stability indicator that is affected by HP and PV integration is transformer overloading TL. More specifically, the 160 kVA transformer has to be replaced from 40% HP integration, and from 60% PV integration.

3.2.2 Cost of low-carbon technologies integration for the low-voltage grid

In this section, we focus on the influence of the combined HP and PV integration on the grid reinforcement cost. For each percentage of HP and PV integration, we select the cost of the cheapest technically viable reinforcement option LCC_d^* in the same way as detailed in Section 3.2.1. The results for the rural and urban grids are provided in Figure 6. In this figure, we also provide the mean of each row ('mean row') and of each column ('mean column').

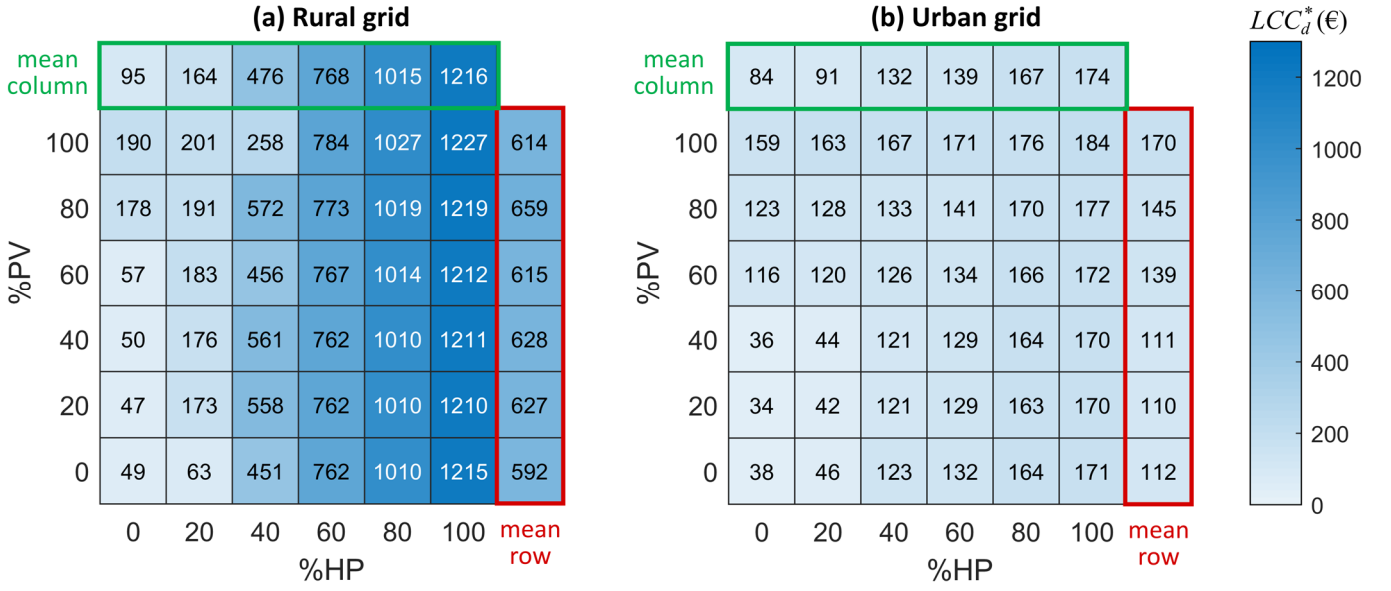

Figure 6 – Influence of the combined HP and PV integration on the cost of the cheapest technically viable reinforcement option LCC_d^*. Rural grid: 68 random repetitions, Urban grid: 27 random repetitions.

In urban areas, for any percentage of integration of both HPs and PV systems, the reinforcement cost remains low (<200 €), as the only required reinforcement is transformer replacement. In rural areas, the small variation along 'mean row' shows that PV integration has a low influence on the cost, while the large variation along 'mean column' highlights that HP integration is the main cost driver. The large cost increase observed from 40% HP integration is due to transformer replacements and to a greater extent to

the re-connection of HPs to three phases for mitigating voltage deviation and unbalance problems (see Section 3.2.1). For 40% HP, we can notice some variations in the reinforcement costs depending on the PV integration, for example lower cost for 100% PV. This is linked to the fact that for this HP integration rate the costs are determined based on few rare voltage violations. Consequently, these may be more easily influenced by the random allocation of LCTs on the grid, and/or potentially remedied with the presence of high levels of PV. However, even though in theory the combined integration of HPs and PV systems could increase grid stability (through the local consumption of PV generation by HPs) and thus decrease grid reinforcement costs, this effect is overall not observed in our case study results for the rural and urban grids. This is notably because the peak in HP consumption occurs during low PV generation periods, namely in the winter during dark hours, while the peak in PV generation occurs at noon during summer.

These results may be compared to some extent with those of McKenna et al. [25], who investigated the integration of HPs and PV systems in low-voltage UK grids. In terms of absolute values, we found a reinforcement cost per dwelling LCC_d^* which reaches up to 1227 €, and which is higher than 1000 € in 17% of the cases. On the other hand, McKenna et al. found a cost per dwelling which reaches up to 3400 € and which is higher than 1000 € in 65% of the cases[1]. These discrepancies may be due to the difference in the considered load profiles and grids. Furthermore, we consider three-phase connection as an additional grid reinforcement option, which is cheaper than feeder replacement in our case. Even though the absolute values differ, McKenna et al. also observed that HP integration was more expensive than PV integration, and that the HP integration cost was larger in rural areas than in urban ones.

3.2.3 Influence of the number of random repetitions

In this section we study the influence of the number of random repetitions ρ on the grid reinforcement cost LCC_d^*. This helps estimating the number of repetitions that should be performed in order to increase the robustness of the results, while minimizing the total computing time (i.e. not performing more repetitions than necessary). The methodology for this analysis is of course applicable to any other case study. The procedure consists in consecutively adding more repetitions and computing the reinforcement costs, until convergence to a predetermined accuracy level is achieved.

First, an initial number of random repetitions are performed, for instance 15. The current number of available repetitions ρ', allows us to compute the currently most accurate estimate of the reinforcement cost for a given LCT integration scenario, denoted $LCC_d^*(\rho')$. Figure 6a gives an example of the resulting $LCC_d^*(\rho')$ for all integration scenarios for the rural grid, which are computed using all $\rho' = 68$ repetitions.

Second, to determine whether the current ρ' is sufficient, for each integration scenario, the relative error made when considering only the first ρ repetitions is computed, for all ρ smaller than ρ':

$$\Delta LCC_d^*(\rho) = \frac{LCC_d^*(\rho) - LCC_d^*(\rho')}{LCC_d^*(\rho')},\ \rho < \rho' \tag{9}$$

Finally, the current number of repetitions ρ' is considered sufficient when $\Delta LCC_d^*(\rho)$ was found smaller in absolute value than a predetermined limit value lim (e.g. $lim = 0.01$), for all LCT integration scenarios and for at least a number ρ_{conv} (e.g. $\rho_{conv} = 10$) of values of ρ before ρ':

$$|\Delta LCC_d^*(\rho)| < lim\ , \forall\ \rho \in [\rho' - \rho_{conv}, \rho'), \text{and } \forall \text{ integration scenario } \rightarrow \rho' \text{sufficient} \tag{10}$$

This means that LCC_d^* has sufficiently converged and that it is unlikely that it will strongly vary when considering additional random repetitions. Otherwise, additional repetitions should be performed until a ρ' is found for which the condition in Eq. (10) is met. Note that the values of lim and ρ_{conv} should be tuned depending on the desired robustness of the results and on the available computing time.

For our case study, considering $lim = 0.01$ and $\rho_{conv} = 10$, convergence is reached for $\rho' = 68$ repetitions in the rural case and $\rho' = 27$ repetitions in the urban case. In Figure 7, the variation of ΔLCC_d^* for all LCT integration scenarios is shown as a function of the number of random repetitions ρ considered, for the finally chosen ρ'. For each number of random repetitions ρ, we present the distribution (grey areas) and the average ΔLCC_d^* between all LCT integration scenarios.

[1] We consider a conversion rate of 1.11 £/€ (rate on 6 July 2020).

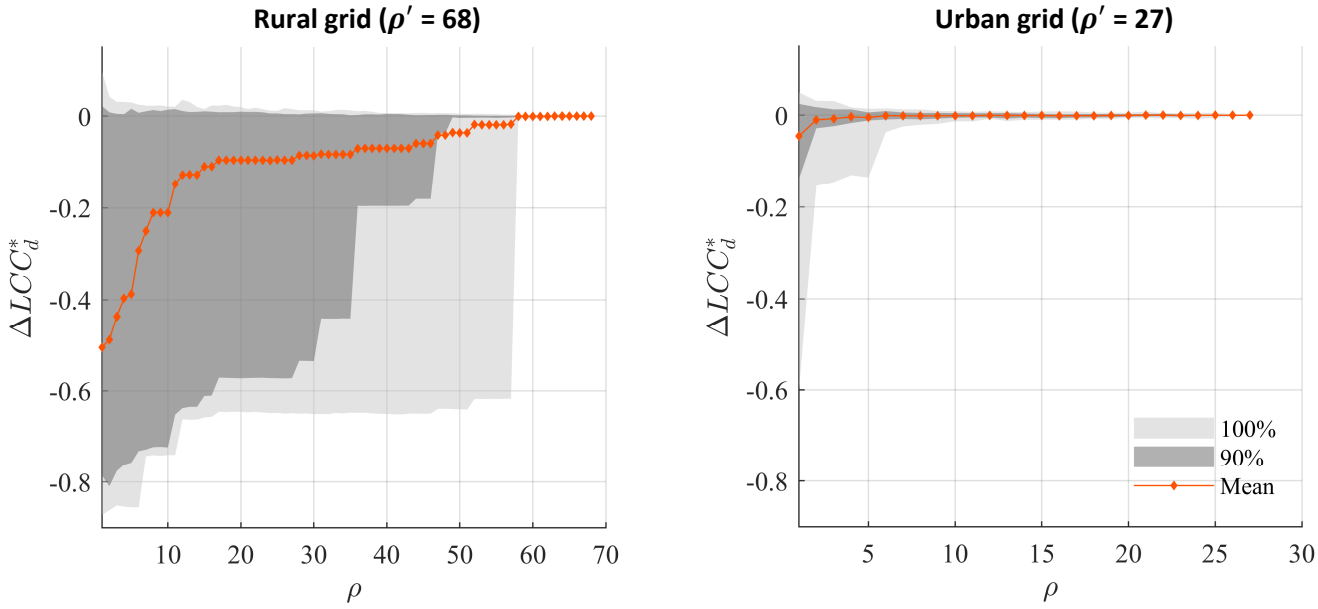

Figure 7 – Influence of the number of repetitions ρ on the grid reinforcement cost. The mean and distribution (grey areas) among all 36 integration scenarios are given for each ρ.

Figure 7 shows that compared to the cost computed for ρ' repetitions, taking fewer repetitions tends to underestimate LCC_d^* ($\Delta LCC_d^* < 0$). Indeed, it may happen that, for a given LCT integration scenario, the random HP and PV positioning in the first random repetitions leads to no grid stability violations for the initial grid. If we were to stop after these first repetitions, no grid reinforcement would be required and the cost LCC_d^* for the LCT integration scenario would be low. However, for the following repetitions the random HP and PV positioning could result in violation of one or several grid stability restrictions. Thus, one or several grid reinforcements would be needed for this LCT integration scenario, which increases the cost LCC_d^*.

Secondly, we observe that ΔLCC_d^* converges faster toward zero for the urban grid than for the rural one. This faster convergence for the urban grid is because, as described in Section 3.2.1, the urban grid only suffers from transformer overloading at high integration levels, while the rural grid has also voltage stability issues (deviation and unbalance). In addition, unlike transformer loading, voltage stability issues are strongly dependent on the positioning of LCTs along the feeder and their distribution across the phases, which varies from one random repetition to another. Thus, contrarily to voltage stability issues, it is more probable that if transformer overloading did not occur for the first repetitions, it will not occur for the following ones.

These results indicate that, when the exact electricity profiles of dwellings are not known and only LCTs integration rates are considered, it is interesting to study the influence of the number of random repetitions on the results in order to improve their robustness while minimizing the computing time. In addition, since the convergence of the reinforcement cost depends on the type and occurrence of grid stability issues, which are related to the grid parameters, it is relevant to perform separate analyses for the different grid types (e.g. urban, rural).

Furthermore, since this methodology considers reinforcements necessary when any repetition encounters grid stability problems, it can be considered as the most conservative approach. A DSO could instead aim to allow a certain probability of grid stability violations, say 5%. This would mean no grid stability violations should occur for 95% of the repetitions, instead of 100%. The definitions of the grid stability indicators could be modified to allow for such a probabilistic assessment.

4 Future work

Even though the methodology has been applied to a specific country and LCTs in this article, it is generic and therefore transferrable to other radial LV grids and LCTs. In the future, we plan to investigate the impact of electric vehicle integration in low-voltage grids, and study the relation of electric vehicles with heat pumps and photovoltaic systems. We also plan to expand the current methodology in order to evaluate the influence of LCT integration on the medium voltage grid. Finally, we will consider mitigation options other than grid reinforcement that also favour the integration of LCTs at the LV level, such as demand side management, reactive power control, and tap changing transformers. Adding these new options to grid reinforcements in the pool of options that can be used to restore grid stability may allow further reducing the grid stabilization cost.

5 Conclusion

In this article, we propose a methodology to identify the low-voltage grid reinforcement options that tackle stability problems, triggered by the integration of residential low-carbon technologies, at the lowest cost. First, a technical model is developed to simulate the influence of low-carbon technology integration scenarios and of grid reinforcement options on four grid stability indicators. This model is able to simulate dynamic behaviour of dwellings, while taking into account stochastic occupant behaviour, and three-phase unbalanced loading of the network. In addition, for the grid simulations we use a dummy island approach, which reduces computing time. This allows performing several random repetitions for a given low-carbon technology integration scenario, thus improving the robustness of our results. Further, we developed an economic model to compute the life-cycle cost associated to a grid reinforcement option, which includes investments and operating costs of the low-voltage grid.

The methodology is applied to investigate the necessary reinforcements to adapt to combined integration of heat pumps and photovoltaic systems in typical rural and urban low-voltage grids of Belgium. We use technical data representative of Belgian dwellings and low-voltage networks, and economic data from a local distribution system operator. For the rural grid, heat pump integration is found to be the main reinforcement cost driver, and may lead to significant reinforcement costs (> 1000 € per dwelling). Indeed, three-phase connection of heat pumps is required to mitigate excessive voltage deviation and unbalance that heat pumps cause in rural grids where feeders are long. For the urban grid, we observe that heat pump and photovoltaic integration causes low reinforcement cost (< 200 € per dwelling), mainly driven by transformer replacement. Finally, we investigate the influence of the number of random repetitions for a given low-carbon technology integration scenario on the robustness of the results. Convergence of the reinforcement cost for urban grids requires fewer repetitions compared to rural grids, leading to reduced computing time. For the rural grid, increased grid stability issues and random effects, such as the location of the low-carbon technologies, cause larger discrepancies between repetitions, meaning that more repetitions are needed to obtain a better understanding of the required grid reinforcements. Overall, the results suggest that, for the considered Belgian case study, it would be more economically efficient, in terms of grid reinforcement, to first deploy heat pumps and photovoltaic systems in urban areas as well as photovoltaic systems in rural ones before integrating heat pumps in rural areas. The methodology proposed in this article can be a useful tool for policy makers and distribution system operators, as it can provide a robust assessment of grid reinforcement cost effectiveness for the integration of low-carbon technologies in the low-voltage grid.

Conflict of interest

None

Acknowledgments

This work is part of the H2020 “sEEnergies” project (https://www.seenergies.eu/). This project has received funding from the European Union’s Horizon 2020 Research and Innovation Action under Grant Agreement No 846463. We would like to thank the reviewers and editors for their thoughtful comments and propositions which allowed to improve the article.

References

[1] N. Good, E.A.M. Ceseña, L. Zhang, and P. Mancarella, “Techno-economic and business case assessment of low carbon technologies in distributed multi-energy systems,” *Appl. Energy*, vol. 167, pp. 158–172, Apr. 2016, doi: 10.1016/j.apenergy.2015.09.089.

[2] G. Carpinelli, F. Mottola, D. Proto, and P. Varilone, “Minimizing unbalances in low-voltage microgrids: Optimal scheduling of distributed resources,” *Appl. Energy*, vol. 191, pp. 170–182, April 2017, doi: 10.1016/j.apenergy.2017.01.057.

[3] A. Navarro-Espinosa and P. Mancarella, “Probabilistic modeling and assessment of the impact of electric heat pumps on low voltage distribution networks,” *Appl. Energy*, vol. 127, pp. 249–266, Aug. 2014, doi: 10.1016/j.apenergy.2014.04.026.

[4] M. Andoni, V. Robu, W.-G. Früh, and D. Flynn, “Game-theoretic modeling of curtailment rules and network investments with distributed generation,” *Appl. Energy*, vol. 201, pp. 174–187, Sept. 2017, doi: 10.1016/j.apenergy.2017.05.035.

[5] H. Ruf, “Limitations for the feed-in power of residential photovoltaic systems in Germany – An overview of the regulatory framework,” *Solar Energy*, vol. 159, pp. 588-660, Jan. 2018, doi: 10.1016/j.solener.2017.10.072

[6] H.S. Das, M.M. Rahman, S. Li, and C.W. Tan, “Electric vehicles standards, charging infrastructure, and impact on grid integration: A technological review,” *Renew. Sustain. Energy Rev.*, vol. 120, art. 109618, March 2020, doi: 10.1016/j.rser.2019.109618

[7] D. Fischer and H. Madani, "On heat pumps in smart grids: A review," *Renew. Sustain. Energy Rev.*, vol. 70, pp. 342-357, Apr. 2017, doi: 10.1016/j.rser.2016.11.182

[8] G.I. Pereira, J.M. Specht, P.P. Silva, and R. Madlener, "Technology, business model, and market design adaptation toward smart electricity distribution: Insights for policy making," *Energy Policy*, vol. 121, pp. 426-440, Oct. 2018, doi: 10.1016/j.enpol.2018.06.018

[9] P. Kohlhepp, H. Harb, H. Wolisz, S. Waczowicz, D. Müller, and V. Hagenmeyer, "Large-scale grid integration of residential thermal energy storages as demand-side flexibility resource: A review of international field studies," *Renew. Sustain. Energy Rev.*, vol. 101, pp. 527-547, March 2019, doi: 10.1016/j.rser.2018.09.045

[10] X. Yan, Y. Ozturk, Z. Hu, and Y. Song, "A review on price-driven residential demand response," *Renew. Sustain. Energy Rev.*, vol. 96, pp. 411-419, Nov. 2018, doi: 10.1016/j.rser.2018.08.003

[11] A. Navarro-Espinosa and L.F. Ochoa, "Increasing the PV hosting capacity of LV networks: OLTC-fitted transformers vs. reinforcements," presented at the 6th IEEE Power & Energy Society Innovative Smart Grid Technologies Conference (ISGT), Washington DC, USA, pp. 1–5, June 2015, doi: 10.1109/ISGT.2015.7131856.

[12] A. Scheidler, L. Thurner, M. Kraiczy, and M. Braun, "Automated grid planning for distribution grids with increasing pv penetration," presented at the 6th Solar Integration Workshop - IEA Task 14 Session, Vienna, Austria, pp. 1-9, Nov. 2016.

[13] T. Stetz, K. Diwold, M. Kraiczy, D. Geibel, S. Schmidt, and M. Braun, "Techno-Economic Assessment of Voltage Control Strategies in Low Voltage Grids," *IEEE Trans. on Smart Grid,* vol. 5, no. 4, pp. 2125-2132, July. 2014, doi: 10.1109/TSG.2014.2320813.

[14] T. Stetz, F. Marten, and M. Braun, "Improved Low Voltage Grid-Integration of Photovoltaic Systems in Germany," *IEEE Trans. on Sustainable Energy*, vol. 4, no. 2, pp. 534-542, Apr. 2013, doi: 10.1109/TSTE.2012.2198925.

[15] W. Biener, K. Dallmer-Zerbe, B. Krug, G. Gust, and B. Wille-Haussmann, "Automated distribution grid planning considering smart grid and conventional grid reinforcement technologies," presented at the International ETG Congress 2015; Die Energiewende - Blueprints for the new energy age, Bonn, Germany, pp. 456–461, Nov. 2015.

[16] A. Procopiou and K. Petrou, "Advanced Planning of PV-Rich Distribution Networks – Deliverable 3: Traditional Solutions," University of Melbourne, Feb. 2020, URL: https://arena.gov.au/knowledge-bank/advanced-planning-of-pv-rich-distribution-networks-deliverable-3-traditional-solutions/ [Accessed: 03-Nov-2020]

[17] J. Flinn and C. Webber, "Customer Distributed Energy Resources Grid Integration Study - Residential Net Zero Net Energy Building Integration Cost," California Public Utilities Commission, Oct. 2017.

[18] K.A.W. Horowitz, F. Ding, B. Mather, and B. Palmintier, "The cost of distribution system upgrades to accommodate increasing penetrations of distributed photovoltaic systems on real feeders in the United States," National Renewable Energy Lab (NREL), Apr. 2018.

[19] G. Celli, F. Pilo, G.G. Soma, R. Cicoria, G. Mauri, E. Fasciolo, *et al.* "A comparison of distribution network planning solutions: Traditional reinforcement versus integration of distributed energy storage," presented at the 2013 IEEE Grenoble Conference, Grenoble, France, pp. 1–6, June 2013, doi: 10.1109/PTC.2013.6652338.

[20] J. van der Burgt, S.P. Vera, B. Wille-Haussmann, A.N. Andersen, and L.H. Tambjerg, "Grid impact of charging electric vehicles; study cases in Denmark, Germany and The Netherlands," presented at the 2015 IEEE Eindhoven PowerTech, Eindhoven, Netherlands, pp. 1–6, July 2015, doi: 10.1109/PTC.2015.7232234.

[21] J. Quirós-Tortós and L.F. Ochoa, "Multi-Year Planning of LV Networks with EVs Accounting for Customers, Emissions and Techno-Economics Aspects: A Practical and Scalable Approach," *IET Generation, Transmission & Distribution*, pp. 1-11, Sept. 2020.

[22] C.K. Gan, M. Aunedi, V. Stanojevic, G. Strbac, and D. Openshaw, "Investigation of the impact of electrifying transport and heat sectors on the UK distribution networks," presented at the 21st International Conference on Electricity Distribution, Frankfurt, Germany, pp. 1–4, June 2011.

[23] S.C. Vegunta, P. Twomey, and D. Randles, "Impact of PV and load penetration on LV network voltages and unbalance and potential solutions," presented at the 22nd International Conference and Exhibition on Electricity Distribution (CIRED 2013), Stockholm, Sweden, pp. 1–14, June 2013, doi: 10.1049/cp.2013.1256.

[24] UK Energy Research Centre (UKERC), "Electricity user load profiles by profile class," Dec. 1997, URL: https://ukerc.rl.ac.uk/DC/cgi-bin/edc_search.pl?GoButton=Detail&WantComp=42&WantResult=LD&&BROWSE=1 [Accessed: 03-Nov-2020]

[25] R. McKenna, P. Djapic, J. Weinand, W. Fichtner, and G. Strbac, "Assessing the implications of socioeconomic diversity for low carbon technology uptake in electrical distribution networks," *Appl. Energy*, vol. 210, pp. 856–869, Jan. 2018, doi: 10.1016/j.apenergy.2017.07.089.

[26] S. Few, P. Djapic, G. Strbac, J. Nelson, and C. Candelise, "Assessing local costs and impacts of distributed solar PV using high resolution data from across Great Britain," *Renew. Energy*, vol. 162, pp. 1140–1150, Aug. 2020, doi: 10.1016/j.renene.2020.08.025.

[27] N.B.G. Brinkel, W.L. Schram, T.A. AlSkaif, I. Lampropoulos, W.G.J.H.M. van Sark, "Should we reinforce the grid? Cost and emission optimization of electric vehicle charging under different transformer limits," *Applied Energy*, vol. 276, pp. 1-13, July 2020, doi: 10.1016/j.apenergy.2020.115285

[28] IEEE, "IEEE PES AMPS DSAS Test Feeder Working Group," 2020, URL: https://site.ieee.org/pes-testfeeders/resources/ [Accessed: 01-Nov-2020]

[29] B. Morvaj, R. Evins, and J. Carmeliet, "Decarbonizing the electricity grid: The impact on urban energy systems, distribution grids and district heating potential," *Appl. Energy*, vol. 191, pp. 125–140, April 2017, doi: 10.1016/j.apenergy.2017.01.058.

[30] R. Baetens, "On externalities of heat pump-based low-energy dwellings at the low-voltage distribution grid," PhD thesis, KU Leuven, Belgium, 2015.

[31] C. Protopapadaki, "A probabilistic framework towards metamodeling the impact of residential heat pumps and PV on low-voltage grids," PhD thesis, KU Leuven, Belgium, 2018.

[32] C. Protopapadaki and D. Saelens, "Sensitivity of Low-Voltage Grid Impact Indicators to Modeling Assumptions and Boundary Conditions in Residential District Energy Modeling," presented at the 15th Conference of the International Building Performance Simulation Association, San Francisco, CA, USA, pp 752-760, Aug. 2017.

[33] J. Van Roy, "Electric Vehicle Charging Integration in Buildings: Local Charging Coordination and DC Grids," PhD thesis, KU Leuven, Belgium, 2015.

[34] L. Lampe, A.M. Tonello, and T.G. Swart, *Power Line Communications: Principles, Standards and Applications from Multimedia to Smart Grid,* 2nd edition, Hoboken, NJ, USA: John Wiley & Sons, 2016.

[35] C. Protopapadaki and D. Saelens, "Towards metamodeling the neighborhood-level grid impact of low-carbon technologies," *Energy Build.*, vol. 194, pp. 273–288, July 2019, doi: 10.1016/j.enbuild.2019.04.031.

[36] R. Baetens, R. De Coninck, F. Jorissen, D. Picard, L. Helsen, and D. Saelens, "Openideas-an open framework for integrated district energy simulations," presented at the 14th Conference of the International Building Performance Simulation Association, Hyderabad, India, pp. 347-354, Dec. 2015.

[37] R. Baetens and D. Saelens, "Modelling uncertainty in district energy simulations by stochastic residential occupant behaviour," *J. Build. Perform. Simul.*, vol. 9, no. 4, pp. 431–447, Sept. 2015, doi: 10.1080/19401493.2015.1070203.

[38] U.S. Department Of Energy, "Heat pump systems," 2020, URL: https://www.energy.gov/energysaver/heat-and-cool/heat-pump-systems [Accessed: 25-Oct-2020]

[39] Vito, "Steunpunt energie: nota potentieel 2030 - warmtepompen," 2017, URL: https://www.energiesparen.be/sites/default/files/atoms/files/Potentieel_warmtepompen_2030.pdf [Accessed: 25-Oct-2020]

[40] R. Baetens, R. De Coninck, J. Van Roy, B. Verbruggen, J. Driesen, L. Helsen, *et al.*, "Assessing electrical bottlenecks at feeder level for residential net zero-energy buildings by integrated system simulation," *Appl. Energy*, vol. 96, pp. 74–83, Aug. 2012, doi: 10.1016/j.apenergy.2011.12.098.

[41] F. Jorissen, G. Reynders, R. Baetens, D. Picard, D. Saelens, and L. Helsen., "Implementation and verification of the IDEAS building energy simulation library," *J. Build. Perform. Simul.*, vol. 11, no. 6, pp. 669-688, Feb. 2018, doi: 10.1080/19401493.2018.1428361.

[42] W. De Soto, S.A. Klein, and W.A. Beckman, "Improvement and validation of a model for photovoltaic array performance," *Solar Energy*, vol. 80, no. 1, pp. 78-88, Jan. 2006, doi: 10.1016/j.solener.2005.06.010.

[43] J. Van Roy, R. Salenbien, and J. Driesen, "Modelica library for building and low-voltage electrical AC and DC grid modeling," presented at the 10th International Modelica Conference, Lund, Sweden, pp 301-309, March 2014, doi: 10.3384/ecp14096301 .

[44] H. Markiewicz and A. Klajn, "Voltage Disturbances; Standard EN 50160 - Voltage Characteristics in Public Distribution Systems," Wroclaw University of Technology, July 2004, URL: http://copperalliance.org.uk/uploads/2018/03/542-standard-en-50160-voltage-characteristics-in.pdf [Accessed: 03-Oct-2020]

[45] A. Navarro-Espinosa and L.F. Ochoa, "Probabilistic impact assessment of low carbon technologies in LV distribution systems," *IEEE Trans. Power Syst.*, vol. 31, no. 3, pp. 2192–2203, July 2015, doi: 10.1109/TPWRS.2015.2448663

[46] T.-H. Chen, C.-H. Yang, and N.-C. Yang, "Examination of the definitions of voltage unbalance," *Int. J. Electr. Power Energy Syst.*, vol. 49, pp. 380–385, July 2013, doi: 10.1016/j.ijepes.2013.02.006.

[47] D. Wu, L. Aye, T. Ngo, and P. Mendis, "Optimisation and financial analysis of an organic Rankine cycle cooling system driven by facade integrated solar collectors," *Appl. Energy*, vol. 185, pp. 172–182, Jan. 2017, doi: 10.1016/j.apenergy.2016.10.071.

[48] 3E, "Aansluiting met flexibele toegang in Vlaanderen - Finaal Rapport Simulatiestudie," May 2017, URL: https://www.vreg.be/sites/default/files/simulatiestudie_aansluiting_met_flexibele_toegang_externe_publicatie.pdf [Accessed: 03-Nov-2020]

[49] Fluvius, "Elektriciteit tariefbladen finaal," 2020, URL: https://www.fluvius.be/sites/fluvius/files/2019-12/fluvius-aansluittarieven-elektriciteit-2020.pdf [Accessed: 03-Nov-2020]

[50] S. Ćurčić, G. Strbac, and X.-P. Zhang, "Effect of losses in design of distribution circuits," *IEE Proc.-Gener. Transm. Distrib.*, vol. 148, no. 4, pp. 343–349, July 2001, doi: 10.1049/ip-gtd:20010359.

[51] C. Protopapadaki and D. Saelens, "Heat pump and PV impact on residential low-voltage distribution grids as a function of building and district properties," *Appl. Energy*, vol. 192, pp. 268–281, April 2017, doi : 10.1016/j.apenergy.2016.11.103.

[52] Synergrid, "Prescriptions techniques spécifiques de raccordement d'installations de production décentralisée fonctionnant en parallèle sur le réseau de distribution - edition 2.1," Sept. 2019, URL :

https://www.sibelga.be/uploads/assets/58/fr/20191104142219000000-Synergrid_Technical_prescription_C10-11_FR.pdf [Accessed: 01-Nov-2020]

[53] R.M. Ciric and M.L.J. Markovic, "Power Factor Analysis in Distribution Network with Roof Photovoltaic Units," *J Electr Eng Electron Technol*, vol. 6, no. 4, p. 1–9, Sept. 2017, doi: 10.4172/2325-9833.1000148

[54] VREG, "Tariefmethodologie voor distributie elektriciteit en aardgas gedurende de reguleringsperiode 2017-2020," Aug. 2016, URL: https://www.vreg.be/sites/default/files/document/tariefmethodologie_reguleringsperiode_2017-2020_2.pdf [Accessed: 03-Oct-2020]

[55] Elexys, "IceEndexPowerBE," Jan. 2020, URL: https://my.elexys.be/MarketInformation/IceEndexPowerBE.aspx [Accessed: 01-Aug-2020]

[56] Meteotest, "Meteonorm Version 6.1 - Edition 2009," 2009, URL: https://meteonorm.com/ [Accessed: 01-Sep-2020]

[57] Inflation.eu, "Inflation moyenne en Belgique (IPC) - par année," 2020. URL : https://fr.inflation.eu/taux-de-inflation/belgique/inflation-historique/ipc-inflation-belgique.aspx [Accessed: 01-Nov-2020]

[58] NBN, "Standard NBN EN 12831 ANB : 2015; Heating systems in buildings - Method for calculation of the design heat load - National annex," June 2015, URL: https://www.nbn.be/shop/en/standard/nbn-en-12831-anb-2015~503927/ [Accessed: 01-Nov-2020]

[59] Dell, "Precision 7910 Tower," 2021, URL: https://www.dell.com/en-us/work/shop/desktops-all-in-one-pcs/precision-7910/spd/precision-t7910-workstation [Accessed: 08-Mar-2021]

[60] Fluvius, "betreffende de aansluitingen op het distributienet laagspanning Un < 1 kV voor afname en injectie van elektrische energie," Jan. 2020, URL: https://www.fluvius.be/sites/fluvius/files/2020-02/aansluitingsreglement-elektriciteit-laagspanning.pdf [Accessed: 02-Nov-2020]